



HAL
open science

Magnetic molecules as local sensors of topological hysteresis of superconductors

Giulia Serrano, Lorenzo Poggini, Giuseppe Cucinotta, Andrea Luigi Sorrentino, Niccolò Giaconi, Brunetto Cortigiani, Danilo Longo, Edwige Otero, Philippe Saintavit, Andrea Caneschi, et al.

► **To cite this version:**

Giulia Serrano, Lorenzo Poggini, Giuseppe Cucinotta, Andrea Luigi Sorrentino, Niccolò Giaconi, et al.. Magnetic molecules as local sensors of topological hysteresis of superconductors. *Nature Communications*, 2022, 13 (1), pp.3838. 10.1038/s41467-022-31320-5 . hal-03824833

HAL Id: hal-03824833

<https://hal.science/hal-03824833>

Submitted on 21 Oct 2022

HAL is a multi-disciplinary open access archive for the deposit and dissemination of scientific research documents, whether they are published or not. The documents may come from teaching and research institutions in France or abroad, or from public or private research centers.

L'archive ouverte pluridisciplinaire **HAL**, est destinée au dépôt et à la diffusion de documents scientifiques de niveau recherche, publiés ou non, émanant des établissements d'enseignement et de recherche français ou étrangers, des laboratoires publics ou privés.

Magnetic molecules as sensors of topological hysteresis of superconductors

Giulia Serrano,^{1*} Lorenzo Poggini,² Giuseppe Cucinotta,³ Andrea Luigi Sorrentino^{1,3}, Niccolò Giaconi,^{1,3} Brunetto Cortigiani,³ Danilo Longo,⁴ Edwige Otero,⁴ Philippe Saintavrit,^{4,5} Andrea Caneschi,¹ Matteo Mannini,^{3*} Roberta Sessoli³

¹ *Department of Industrial Engineering (DIEF) and INSTM Research Unit, University of Florence, Via Santa Marta 3, 50139 Florence, Italy. giulia.serrano@unifi.it*

² *Institute for Chemistry of Organo-Metallic Compounds (ICCOM-CNR), Via Madonna del Piano 10, 50019 Sesto Fiorentino (FI), Italy.*

³ *Department of Chemistry "U. Schiff" (DICUS) and INSTM Research Unit, University of Florence, Via della Lastruccia 3-13, 50019 Sesto Fiorentino (FI), Italy. matteo.mannini@unifi.it*

⁴ *Synchrotron SOLEIL, L'Orme des Merisiers, 91192 Saint-Aubin, France.*

⁵ *Institut de Minéralogie, de Physique des Matériaux et de Cosmochimie (IMPMC), CNRS, Sorbonne Université, 4 place Jussieu, 75252 Paris Cedex 5, France.*

Abstract

Superconductors and magnetic materials, including molecules, are key ingredients for quantum and advanced spintronic applications. However, only a little is known about how these materials are mutually influenced at their interface in hybrid architectures. Here, we show that a single layer of magnetic molecules, the Terbium(III) bis-phthalocyaninato (TbPc₂) complexes, deposited on a superconducting Pb(111) surface is sensitive to the topology of the intermediate state of the superconductor, namely to the presence and evolution of superconducting and normal domains due to the magnetic field screening and penetration. The evidence of this sensitivity is found in the magnetisation dynamics of the TbPc₂ sub-monolayer in its paramagnetic regime showing the fingerprint of the topological hysteresis of the superconducting substrate. This study reveals the great potentialities hold by thin layers of magnetic molecules for sensing local magnetic field variation in hybrid molecular/superconductor architectures, including spin resonators or spin injection devices for spintronics applications.

Introduction

Recently, the coupling between magnetic materials and superconductors (SCs) has raised an increasing interest for its potentialities in spintronics and quantum technologies.^{1,2} First, their coupling led to an enhancement of spintronic related phenomena, such as spin injection and magnetoresistance.¹ At the nanoscale, the interaction of single spins with superconducting substrates revealed the appearance of local bound states within the SC band gap^{3,4} opening a route to

35 creating Majorana bound states which may be used as fundamental units for topological quantum computing
36 applications.⁵ Differently from individual atoms or bulk impurities, magnetic molecules profit from a well-defined
37 chemical structure that can be engineered to tune the molecular spin coupling strength with superconducting substrates
38 and control local bound states.⁴ From a technological point of view, the realization of hybrid molecular –
39 superconductor architectures can permit the integration of molecular qubits in quantum circuit, as superconducting
40 microwave resonators,^{6,7} or to produce dissipationless spin currents through spin singlet-to-triplet conversion
41 mechanism.⁸

42 An important step forward in the research on hybrid materials comprising molecules and superconductors was
43 achieved by some of us, depositing a single layer of single molecule magnets (SMMs) retaining their magnetic memory
44 on Pb(111). It was shown that the transition of Pb to the superconducting state alters the magnetization dynamics of the
45 Fe₄ SMMs complexes inducing a switching of their magnetic state from a blocked state to a resonant regime via
46 quantum tunnelling of the magnetization.⁹ This phenomenon was observed for the first time in the magnetic hysteresis
47 loop of the SMMs layer recorded by synchrotron radiation and indicated that the superconducting transition may
48 severely influence the magnetic properties of the molecular film at a large scale. Besides these seminal results, a deep
49 understanding of the key ingredients characterizing the interface between molecules and superconductors was necessary
50 to explore the frontiers of the molecular sensitivity to the superconducting state. For this reason, here we growth on top
51 of a Pb(111) single crystal a layer of a more anisotropic SMM, the Terbium(III) bis-phthalocyaninato (TbPc₂) complex,
52 that is known to significantly interact with the metallic surfaces.^{10–12} TbPc₂ is a double-decker system formed by two
53 phthalocyanines (Pc) coordinating a Tb^{III} ion^{13–17} (**Figure 1a**). The complex is characterized by a strong uniaxial
54 anisotropy with the easy axis of the magnetization oriented perpendicularly to the Pc planes (**Figure 1a**). Near liquid
55 helium temperatures and in bulk crystals, it behaves as a single molecule magnet thanks to the large energy barrier
56 separating the ground doublet states
57 ($J_z = \pm 6$) that hinders the reversal of the magnetization. At variance with Fe₄ SMM complexes,^{18,19} both the electronic
58 and magnetic properties of TbPc₂ are particularly sensitive to the interaction with substrates. The signature of this
59 interaction was observed on a wide range of metallic and non-metallic substrates either at the single molecule level or at
60 the larger scale of the molecular film.^{20–22} Remarkable effects were found in the magnetic hysteresis loop of TbPc₂
61 films, which is quenched for molecules directly interacting with metals while preserved or improved by the use of
62 decoupling layers^{21–23} or anchoring groups.²⁴ Small apertures of the hysteresis loop were found only for TbPc₂
63 monolayer on TiO₂ films,²⁵ graphene²¹ or HOPG²⁶ substrates. On the other side, MgO films separating the TbPc₂ from
64 the metal Ag(100) surface, led to large magnetic remanence and the disappearance of the quantum tunnelling of the
65 magnetisation at zero field.²²

66 The sensitivity of TbPc₂ films to the environment has been here exploited to investigate the magnetization of
67 TbPc₂ at the interface with Pb(111) and across its superconducting transition, as a function of the temperature and
68 magnetic field. To achieve this purpose, we deposited by thermal sublimation a sub-monolayer of TbPc₂ molecules
69 directly on Pb(111). The study, performed by *in house* surface characterization methods (*e.g.* Scanning Tunnelling
70 Microscopy, STM, and X-ray Photoelectron Spectroscopy, XPS) and synchrotron radiation, showed that the
71 magnetization curve of the investigated TbPc₂ sub-monolayer is influenced by the topology of the superconducting and
72 normal domains of Pb when the magnetic field intensity is raised or lowered. This effect causes the opening of the
73 hysteresis loop of TbPc₂ within the superconducting regime of the substrate, which is ascribed to the topological
74 hysteretic behaviour of the substrate.

75

76 Results

77 The Pb(111) crystal was prepared according to the procedure reported in the Methods and preliminarily characterized
78 by

79 XPS and STM (see **Figure S1**). The molecular deposit on Pb(111) was obtained by thermal sublimation of the TbPc₂
80 powder dosing a sub-monolayer amount (see Methods). The growth and adsorption configuration of TbPc₂ on Pb(111)
81 was studied by STM at low temperature (35 K) and low surface coverage (~ 30%). **Figure 1b** shows a 3D STM image
82 of the TbPc₂ sub-monolayer on Pb(111). The image shows large Pb(111) terraces with monoatomic steps (indicated by
83 yellow arrows) of about 0.3 nm height.⁹ The black arrow indicates an island of TbPc₂ molecules deposited on the clean
84 Pb(111) surface. The formation of regular islands is common for the deposition of TbPc₂ thin films on many other
85 surfaces.^{22,27,28} The height of the island is about 0.5 nm, consistently with the distance between the two Pc planes. This
86 also indicates that the molecules maintain the lying down configuration (Pc planes parallel to the surface), mostly
87 observed on metal surfaces.^{21,22,27,28} The TbPc₂ sub-monolayer on Pb(111) was characterized by XPS at room
88 temperature to study the molecular stoichiometry and interaction with the substrate (see Methods) evidencing spectral
89 features (**Figures 1c and d and Figure S2**) in line with those observed for monolayer or thick films on other
90 surfaces.²⁹⁻³¹ The *Cl*s spectrum of the TbPc₂ film on Pb is characterized by two main components at 284.5 eV and
91 285.4 eV ascribed to C-C and C-N bonds, and related shake-up signals at 286.4 eV and 288.0 eV.^{29,30} The *NI*s spectrum
92 shows the main component at 398.5 eV and a shake-up at 400.4 eV.²⁹⁻³¹ In **Figure S2** are also reported the XPS Pb*4f*
93 spectrum after molecular deposition, showing the Pb*4f*_{7/2} calibrated at 136.9 eV, and the Tb*3d* region, showing the *3d*_{3/2}
94 signal at 1276 eV.^{9,30,32,33} We remark that the Tb*3d*_{5/2} signal overlaps with the Auger lines of Pb and C, α-N₆O_{4,5}O_{4,5} and
95 KVV,³⁴ respectively, and it cannot be used for quantitative analysis. However, the C/N XPS signal ratio is 3.8, in close

96 agreement with that expected from the molecular stoichiometry ($C/N_{\text{theory}} = 4$) and indicates the integrity of the
 97 molecular layer.

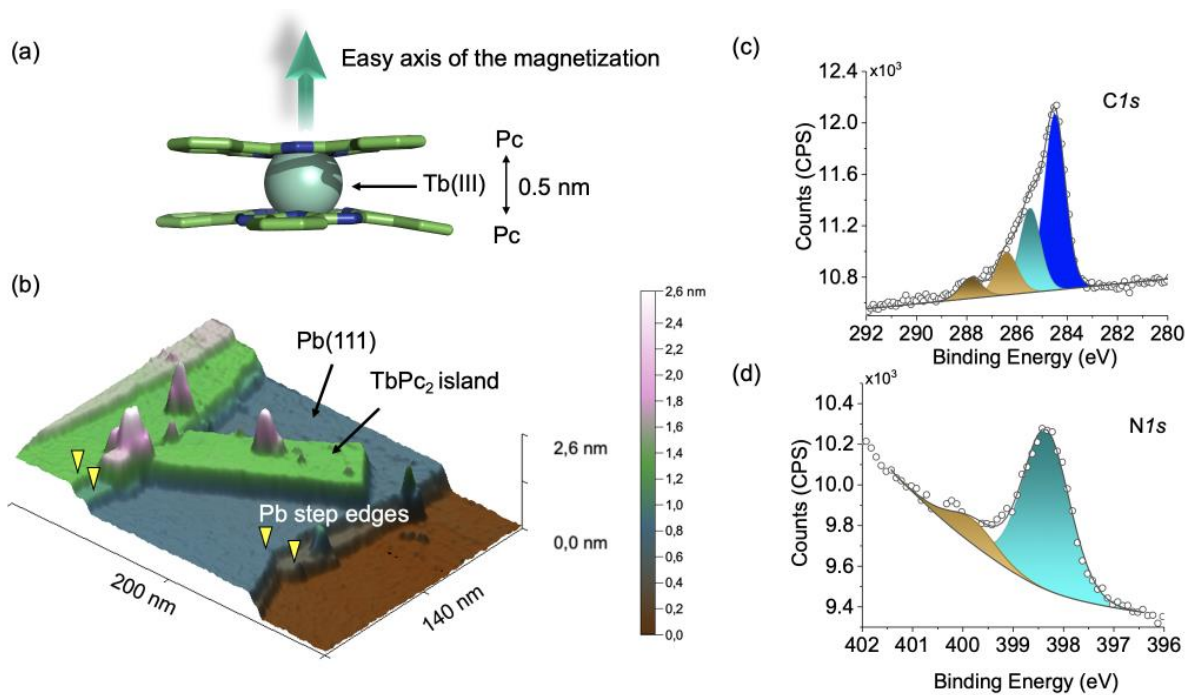


Figure 1. Structural characterization of the TbPc₂ sub-monolayer on Pb(111). (a) Scheme of the TbPc₂ structure. Colour code: green, carbon; blue, nitrogen; light cyan, terbium, hydrogens are omitted for clarity. The easy axis of the magnetisation is directed perpendicularly to the phthalocyanine (Pc) planes and sketched by an arrow. (b) 3D STM image of a TbPc₂ island on Pb(111) recorded at 35K ($I_{\text{tunnel}} = 5$ pA, $V_{\text{bias}} = 2$ V). The Z-colour scale is shown on the right. (c) C1s and (d) N1s XPS core-level spectra of the TbPc₂ sub-monolayer on Pb(111). Main components are shown in blue and cyan; shake-up components are shown in brown.

98 Synchrotron characterization was performed to investigate the magnetic properties of the TbPc₂ sub-monolayer
 99 on Pb(111) by X-ray Absorption Spectroscopy (XAS), see **Figure 2a-c**. All the measurements were recorded in the
 100 Total Electron Yield (TEY) mode (see Methods) with the magnetic field and X-ray beam axis at an angle θ from the
 101 sample's surface normal (see inset **Figure 2b**). XAS spectra were recorded using the positive (σ^+) and negative (σ^-)
 102 circular polarisation of the X-ray light to obtain the X-ray Magnetic Circular Dichroism (XMCD) spectrum ($\sigma^- - \sigma^+$) at
 103 the Tb M_{4,5} edges. **Figure 2a** shows the XAS and XMCD spectra recorded at normal incidence ($\theta = 0^\circ$), 2 K and 3 T.
 104 The XMCD intensity value is normalised respect to the edge jump value of the isotropic XAS spectrum (see Methods).
 105 The strong dichroic signal at the M₅ edge, 1237 eV, has an intensity of about 140%, in good agreement with TbPc₂
 106 monolayer and thick films previously investigated.²⁰⁻²⁴ Indeed, this XMCD spectrum is representative of saturated Tb^{III}
 107 ions with total angular momentum $J = L + S = 6$ and in the symmetry imposed by the two Pc ligands.^{20,35} At $\theta = 45^\circ$, the
 108 intensity of the XMCD signal slightly decreases to about 120% (see **Figure S3 (a)**) as a consequence of the uniaxial
 109 anisotropy of TbPc₂ molecules that are oriented with their easy axis of magnetisation perpendicular to the surface.²⁰ In
 110 **Figure S3(b)** and (c) are also reported the XMCD spectra recorded for $\theta = 0^\circ$ and 3T at 4K and 8 K, respectively,

111 which show the preservation of the strong dichroic signal at 1237 eV of the M_5 edge, as expected for a sub-monolayer
 112 coverage.^{20–24}

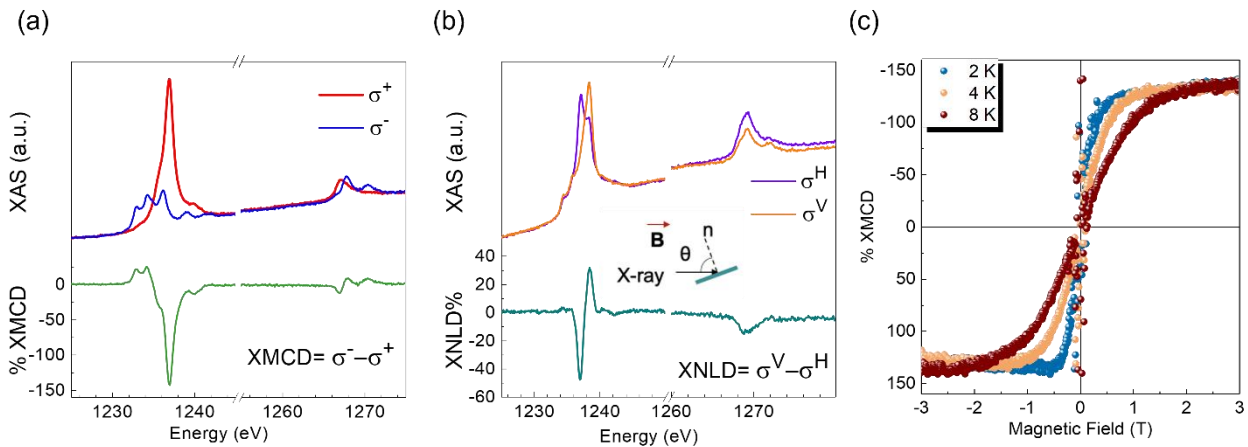


Figure 2. Magnetic characterisation of the TbPc₂ monolayer on Pb(111). (a) XAS and XMCD spectra recorded at $\theta = 0$, 2 K and 3 T. (b) XAS and XNLD spectra recorded at $\theta = 45$, 2 K and 3 T. (c) Magnetic hysteresis loop recorded at $\theta = 0$ and at different temperatures (2K, blue; 4K, orange; 8 K, red).

113 At $\theta = 45^\circ$, XAS spectra were also recorded using linear vertical (σ^V) and horizontal (σ^H) light polarisation,
 114 whose difference ($\sigma^V - \sigma^H$) provides the X-ray Natural Linear Dichroism (XNLD) spectrum. The XNLD contribution
 115 gives information about the alignment of molecules in the layer and it can be used to determine the orientation of TbPc₂
 116 molecules on the surface.^{20,21} The XNLD spectrum for the TbPc₂ sub-monolayer on Pb(111), expressed in percentage
 117 according to the formula reported in the Methods, is shown in **Figure 2b**. The shape of the dichroic signal, presenting a
 118 minimum at 1237 eV with an intensity of about -50%, is a confirmation of the lying down orientation of the molecules
 119 in the monolayer, and a narrow distribution of the orientation similarly to highly oriented TbPc₂ films on graphene and
 120 gold substrates.^{20,21}

121 Magnetic field dependence of the XMCD signal at the Tb M_5 edge, 1237 eV, and before the pre-edge value,
 122 1225eV, was measured to extract the trend of the normalized XMCD while sweeping the magnetic field (see Methods)
 123 and follow the magnetic behaviour of the absorber. **Figure 2c** shows the trend obtained scanning magnetic field
 124 directed perpendicular to the sample surface ($\theta = 0^\circ$) with a scan rate of 0.02 T/s from -3T to 3T and vice versa. The
 125 figure shows the temperature dependence of these loops at 8 K, 4 K and 2 K (the error on the temperature value is
 126 estimated to be less than 10% of the value). As expected, given the magnetic anisotropy of the investigated sample, by
 127 decreasing the temperature increases the steepness of the curves at low fields, and decreases the field at which
 128 saturation is reached. At 2 K, the dichroism at saturation is about 140%, coherently with the intensity of the maximum
 129 dichroic signal in the XMCD spectrum recorded at 3 T and shown in **Figure 2a**. At all temperatures, the expected
 130 opening due to the SMM behaviour is quenched, and TbPc₂ molecules act as paramagnets. This behaviour is typical of
 131 monolayers of TbPc₂ deposited on metals.^{12,20,22,23,36} On the other hand, the interest in this magnetic

132 molecule/superconductor hybrid resides in the sensitivity given by the strong uniaxial magnetic anisotropy of the TbPc₂
 133 complex to the superconducting transition.

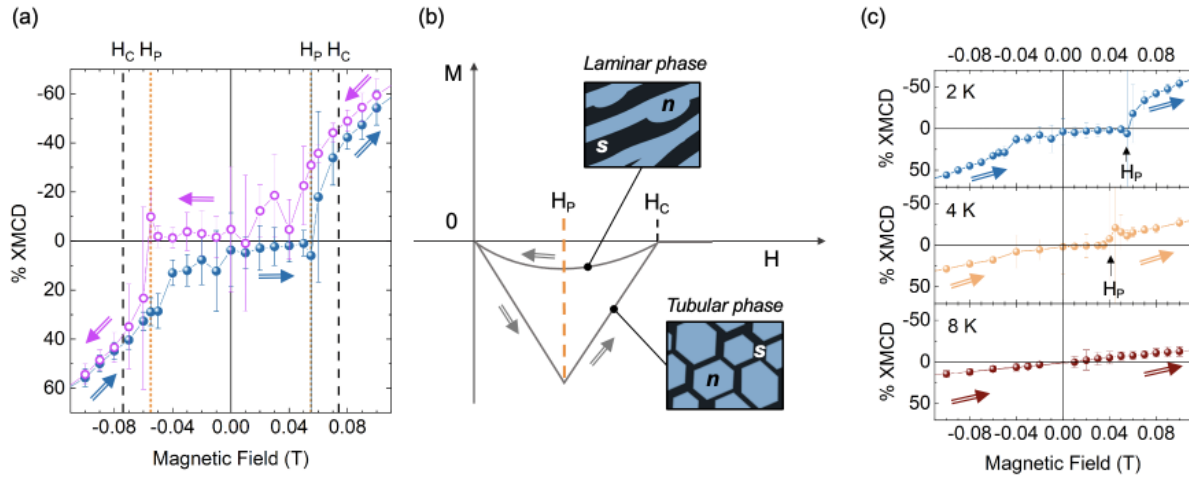


Figure 3. Magnetic behaviour of the TbPc₂ sub-monolayer on Pb(111) across the superconducting transition.

(a) Magnetisation curves of TbPc₂ monolayer on Pb(111) at 2K and $\theta = 0^\circ$ within the critical field of the superconductor (H_C). The complete magnetic field screening effect of Pb is observed for increasing magnetic field intensity within a certain field H_P . Symbol code: up branch, filled circles; down branch, empty circles; arrows indicate the field scan direction. (b) Sketch of a typical magnetisation loop of disk shaped Pb single crystals (see Ref. ⁴¹). The hysteresis loop of bulk Pb crystals originates from the different topology of the intermediate state when the magnetic flux penetrates or is expelled from the substrate. The topology (tubular and laminar) of the micrometric superconducting (s) and normal (n) domains in the intermediate state depicted in the figure is representative of the magneto-optical images of Pb crystals of Ref. ⁴¹. (c) Magnetization curve (up branch) of TbPc₂ on Pb(111) for $\theta = 0^\circ$ at different temperatures below (2 K and 4K) and above (8 K) the critical temperature.

134 The Pb(111) substrate is superconductive below its critical temperature, $T_C = 7.2 K$, and within the critical
 135 field value H_C that varies with the temperature according to the formula $H_C(T) = H_C(0)[1 - (\frac{T}{T_C})^2]$ (1).³⁷
 136 Being $H_C(0) = 0.08 T$ for Pb,³⁸ H_C is expected to be at 0.074 T at 2 K. Thus, is in the previous measurements
 137 (**Figure 2c**) the magnetic field region within H_C is hidden below the limit of the scan resolution adopted and below the
 138 strong noise of the XMCD signal detected by the TEY when the field is swept across zero.

139 To overcome this limitation, instead of acquiring the TEY signal during a magnetic field sweep, magnetisation
 140 curves were collected for each X-ray light polarization by integrating over time the TEY signal at each sampled field
 141 (see Methods). **Figure 3a** shows that at 2K, the trend of the TbPc₂ XMCD signal within the superconducting regime of
 142 Pb, is strongly influenced, presenting an hysteretic behaviour. We observe that by decreasing the magnetic field
 143 intensity below the Pb critical field ($|H_C| = 0.072 T$), the XMCD values of TbPc₂ follows an almost linear trend. In this
 144 region the effect of the superconducting transition in the TbPc₂ magnetization curve is therefore negligible, indicating
 145 that the magnetic field is only partially screened by the superconductor. However, after crossing zero field and
 146 increasing the magnetic field intensity, the XMCD values are zero (within the error limits) until a certain field $|H_P| =$
 147 0.055 T. This suggest that, on the contrary, in this regime the magnetic field is completely screened out by the Pb

148 substrate. By increasing the field above H_p , the XMCD values suddenly increase, as the superconductor is back in a
149 regime where only partial magnetic field screening occurs before it turns into the normal state at H_C .

150 The fact that the TbPc_2 XMCD trend of **Figure 3a** shows a hysteretic behaviour is the signature of the
151 transition of the $\text{Pb}(111)$ crystal to the superconducting state and – in particular – of different topology of the normal (n)
152 and superconducting (s) domains when the magnetic flux is penetrating or exiting the superconductor. It is well-
153 established that type I superconductors below their critical field, H_C , and critical temperature, T_C , are characterized by
154 an intermediate state (IS) in which both s (where the magnetic field is completely expelled) and n domains (where the
155 magnetic field penetrates) coexist at the micrometric scale.^{37,39–43} The topology, *i.e.* the shape of these domains,
156 strongly differs during the increase (magnetic flux penetration phase) or decrease (magnetic flux expulsion phase) of the
157 magnetic field intensity. This effect was observed by magneto-optical (MO) images for various type I SCs metals,^{39,44}
158 including Pb crystals.^{37,40,41} The combination of MO and SQUID measurements demonstrated that the topological
159 variation of the IS domains causes a hysteretic behaviour (topological hysteresis).^{37,40,41} In particular, Prozorov⁴¹ treated
160 the case of disk-shaped Pb crystals (of shape and dimensions comparable with the Pb substrate used here) in an axial
161 magnetic field (*i.e.*, along the cylinder axis).

162 A clear interpretation of the TbPc_2 hysteresis at 2.0 K shown in **Figure 3a** can be indeed achieved by
163 comparing the magnetization curves of TbPc_2 film in light of the magnetization curves of Pb crystals reported by
164 Prozorov⁴¹ and here sketched in **Figure 3b**. We remark that the X-ray beam used for the measurements of **Figure 3a**
165 has a spot diameter of about 800 μm that averages over s and n domains of micrometric size and that it is positioned at
166 the centre of the crystal during the measurements. Following the curve sketched in **Figure 3b**, by decreasing the field
167 below H_C , *i.e.* during the magnetic flux expulsion, the magnetisation curve of the Pb crystal shows small magnetisation
168 absolute values, poorly affecting the magnetisation of TbPc_2 whose trend is only slightly deviated from linearity below
169 H_C (see **Figure 3a**). According to Prozorov,⁴¹ in these conditions the s and n domains of the Pb crystal show a *laminar*
170 *topology* (see the sketch in **Figure 3b**). The magnetic flux can exit the sample only through the n domains which shrink
171 on lowering the magnetic field intensity until reaching zero field, where the substrate is completely superconducting,
172 and the magnetic flux is completely excluded (Meissner state). It is worth noticing that when the intermediate state has
173 a laminar topology, the magnetic flux is never fully screened by the superconductor until the external magnetic field is
174 zero. By increasing the magnetic field intensity from zero, the magnetic field does not penetrate the bulk of the sample
175 which remains in an almost diamagnetic state until H_p (negative linear slope in **Figure 3b**).^{41,45} In these conditions
176 magnetic flux can only enter at the edges of the Pb disks but cannot migrate towards its centre,^{41,45} which justifies the
177 overall zero XMCD values detected on the TbPc_2 layer when the field is increased from zero to $|H_p| = 0.055 \text{ T}$. When
178 magnetic field is increased above H_p , magnetic field penetrates through n domains that expand from the sample edges

179 over whole substrate with a *tubular topology*, where an hexagonal symmetry is favoured (see the sketch in **Figure**
180 **3b**).⁴¹ In this phase, TbPc₂ molecules acting as sensors feel an increasing XMCD signal due to the expansion of the *n*
181 domains (**Figure 3a**). We remark that in the intermediate state the magnetic field intensity in normal regions is always
182 equal to H_C^{37,45} and that the increasing of the XMCD intensity here detected is only due to the average over *n* domains
183 of increasing extension. Furthermore, we notice that the XMCD error bar amplitude is maximum at the onset of field
184 penetration in tubular topology; this effect is not observed at the entrance of the SC state (field exclusion onset), where
185 TbPc₂ is already magnetized. The same behaviour was found in the hysteresis curve of Fe₄ complexes on Pb,⁹ and it
186 could be ascribed to the abrupt change in the local magnetic induction of the TbPc₂ molecules (and of the
187 photoelectrons and secondary electrons of the TEY signal) when exiting the demagnetized condition.⁹

188 The hysteretic behaviour of the TbPc₂ XMCD signal shown in **Figure 3a** is maximum at H_p , and the XMCD
189 values are null at zero field, compatibly with the topological hysteresis curves of the SC and further indicating that the
190 hysteresis loop is not a consequence of flux pinning inside the superconductor.⁴¹ We remark that the topological
191 hysteretic behaviour of Pb could not have been previously observed with Fe₄ complexes, due to their SMM properties.⁹
192 The strong drop of the Fe₄ magnetization value observed during magnetic field screening, *i.e.* lowering the magnetic
193 field intensity below H_c, was a consequence of the average decrease of the magnetic field intensity felt by the
194 molecules that performed the quantum tunnelling of the magnetization on *s* regions of increasing width. On the
195 contrary, Fe₄ molecules could not be sensitive to the onset of field penetration (and exit from the superconducting state)
196 since in this field range they could not be magnetized until the first field-induced level crossing was reached.⁹ The
197 paramagnetic character of TbPc₂ allows an enhanced sensitivity to the magnetic flux variation on the surface of the
198 superconductor also in this field region.

199 A closer look to the magnetisation curve of **Figure 3a**, further support our interpretation. Indeed, the onset of
200 the field penetration inside the superconductor varies with the geometry of the superconducting sample, which
201 determines its demagnetizing factor (N). Being $H_p = (1 - N)H_C$ ^{37,41} (2) and considering the experimental H_p value
202 observed in the hysteresis loop at 2 K, we derive an N value for our Pb crystal of about 0.25. This value compares well
203 with that extracted by Prozorov (N=0.55),⁴¹ taking into accounts the different thickness-to-width ratio of the two
204 substrates.⁴⁶

205 **Figure 3c** compares the magnetisation curve of TbPc₂ on Pb(111) - up branch - recorded at 2 K, 4 K and 8 K.
206 The curves show for negative fields the magnetic field expelled from the superconductor and at positive fields, the
207 magnetic field entry. It is evident that the H_p field, *i.e.* the onset of the field penetration, changes with the temperature
208 (at 4 K and 2 K) while it cannot be identified at 8 K. According to equation (1) and (2), at 4.2 K, H_C is expected at
209 0.053 T, and H_p at 0.04 T assuming N = 0.25. The XMCD data at 4 K perfectly support this hypothesis. Finally, the

210 magnetisation curve at 8 K does not evidence the signature of the superconducting transition since it is recorded above
211 the T_C value. The latter evidence, further demonstrate the sensitivity of a single layer of $TbPc_2$ molecules to the
212 superconducting transition.

213 **Conclusions**

214 In conclusion, we deposited a single layer of $TbPc_2$ molecules by thermal sublimation in ultra-high vacuum on
215 a clean Pb(111) surface and we characterized their interface properties by XPS and STM to check the molecular film
216 growth and stoichiometry. Synchrotron light was used to address the magnetic behaviour and the molecular ordering of
217 the $TbPc_2$ film on a on a millimeter range by XMCD and XNLD, respectively. X-ray detected magnetisation
218 measurements performed at the Tb edge showed that the $TbPc_2$ monolayer behaves as a paramagnet when the substrate
219 is in the normal state, as typically observed for monolayer deposits on metal surfaces. However, an opening of the
220 hysteresis loop was observed below the transition of Pb to the superconducting state. We ascribe this phenomenon to
221 the topological hysteresis loop of the superconducting Pb(111) surface, due to the different shape of superconducting
222 and normal domains during magnetic field penetration or expulsion. Further, from the analysis of the superconductor
223 hysteresis loop probed by the molecules and its temperature dependence we derived the critical field and the
224 geometrical factors of the Pb crystal that characterized the transition to the condensate state.

225 At variance with Fe_4 SMMs complexes,⁹ we showed here that a single layer of magnetic molecules can be
226 sensitive not only to the transition to the superconducting state but also to the topological features of superconducting
227 domains. We stress that such sensitivity was achieved on a single layer of $TbPc_2$ in its paramagnetic regime in direct
228 contact with the Pb substrate, which opens the perspective of using the plethora of molecules with spin properties
229 (including highly coherent systems^{47,48}) for detecting superconductivity on a large scale. Thus, $TbPc_2$ is a peculiar probe
230 thanks to the strong magnetic anisotropy and out-of-plane magnetic susceptibility and to the capabilities to form highly
231 oriented films that make them extremely sensitive to local magnetic flux variation.

232 Looking this observation form another point of view, we also demonstrated that the intrinsic topology of the
233 intermediate state of the superconductor can induce a hysteretic behaviour in an ensemble of paramagnetic molecules.
234 This last outcome might have a great potential for technological applications. Furthermore, these results are significant
235 also for those fields that exploit hybrid molecular/superconductor systems in macroscopic devices, as resonators,^{6,7} or
236 for the detection of localised states occurring at the interface between single spins and superconducting surfaces,⁴ where
237 magnetic field screening effects can play an important role.

238 **Methods**

239 The Pb(111) single crystal was acquired from the Surface Preparation Laboratory (SPL) and it had a disk shape
240 with a diameter of 4 mm and a height of 2 mm. The surface was prepared in ultra-high vacuum (UHV) by sputtering
241 cycles of Ar⁺ at 1500 eV and annealing at 473 K for 30 min. Before molecular deposition, surface cleanliness was
242 checked by XPS and STM measurements at room temperature (RT). The molecular deposition was performed by
243 thermal sublimation of the molecular powders using a homemade effusion cell. The sublimation temperature of TbPc₂
244 was 710 K and the flux was estimated by a quartz microbalance. Surface coverage was checked by STM using an
245 Omicron VT-STM with a W tip. STM measurements were carried out by cooling down the sample to 35 K with a
246 helium flux to reduce molecular mobility on the surface.

247 XPS measurements were carried out using a monochromatic Al K α radiation ($h\nu = 1486.6$ eV, SPECS mod. XR-MS
248 focus 600) and a SPECS Phoibos 150 IDLD electron analyser mounted at 54.44° with respect to the X-ray beam. XPS
249 measurements were performed at normal emission with the pass energy set to 40 eV. Spectra were analysed using the
250 CasaXPS software and calibrated at the Pb4f_{7/2} signal at 136.9 eV (see Figure S2, ESI). Spectra were fitted with a linear
251 or Tougaard background⁴⁹ and single-peak components were deconvoluted using a mixed Gaussian and Lorentzian
252 function (70/30). All the above-mentioned *in house* characterizations were performed on the very same sample without
253 breaking the vacuum.

254 X-ray absorption spectroscopy (XAS) experiments were carried out at the DEIMOS beamline, synchrotron SOLEIL
255 (Saint-Aubin, France).⁵⁰ All samples were prepared and characterized in Florence and transferred to the end-station
256 using a UHV suitcase ($P_{\text{base}} = 5 \cdot 10^{-10}$ mbar). XAS spectra were recorded in total electron yield (TEY) mode⁵¹ using both
257 linear and circularly polarized light⁵¹ in a temperature range between 8.0 ± 0.2 and 2.0 ± 0.1 K and magnetic field
258 within ± 3 T (measurements' parameters are specified in the text). XAS spectra were recorded at the Tb M_{4,5} edges at
259 angles θ , defined as the angle between the k X-ray propagation vector and the surface normal. XMCD spectra were
260 normalized to the M₅ edge jump of $(\sigma^+ + \sigma^-)/2$ and expressed in percentage (% XMCD), while XNLD spectra at $\theta=45^\circ$
261 were normalized to the M₅ edge jump of the isotropic spectrum ($\sigma^{\text{iso}} = 1/3\sigma^V + 2/3\sigma^H$) and expressed in percentage (%
262 XNLD).⁵² XAS and dichroic spectra were calibrated by setting the maximum of the XMCD and XNLD at the Tb M₅
263 edge to 1237 eV. Magnetic hysteresis curves were obtained by recording the field dependence of the % XMCD at the
264 Tb M₅ edge (measured at 1237 eV and here referred to the pre-edge dichroism at 1225 eV) sweeping the magnetic field
265 between -3 T and 3 T with a scan rate of 2 T/s. Data treatment for XMCD, XNLD and hysteresis was performed
266 employing the program pyDichroX.⁵³ To avoid the noise present in the TEY signal during the field sweeping when the
267 magnetic field is close to zero, the magnetic hysteresis at low field intensities (**Figure 3**) were acquired by recording the
268 TEY signal at each sampled field and for each X-ray light polarization (circular left and right) using a time-scan
269 acquisition (scan time 120 s with 0.2 s of integration time for a total of 600 data points). This procedure was adopted for

270 both the edge and pre-edge energies to get the normalised dichroic signal. The XMCD values and the associated error
271 bars reported in the hysteresis of **Figure 3** were then obtained considering the average of TEY signal at each field,
272 polarization and energy and the relative standard deviation.

273

274 **Acknowledgements**

275 We thank for the financial support the European COST Action CA15128 MOLSPIN and the FET Open FATMOLS
276 project, Italian MIUR for “Progetto Dipartimenti” di Eccellenza 2018-2022 (ref. no. B96C1700020008), Regione
277 Toscana POR CreO FESR 2014-2020- SENSOR, and Fondazione Cassa di Risparmio di Firenze (Project SPINE-2
278 2020.1634). We acknowledge SOLEIL for the provision of the synchrotron radiation facilities. We thank P. Ohresser
279 and L. Joly for assistance in using the DEIMOS beamline (project 20201244).

280

281 **Author contributions**

282 G.S., L.P., A.L.S., and B.C. prepared the sample and performed in house characterization. G.S., L.P. A.L.S., G.C.,
283 N.G., D.L., M.M., P.S. and E.O. performed synchrotron experiments. G.S., L.P., and G.C. performed and discussed the
284 experiments. G.S. drafted the manuscript. A.C., R.S. P.S. and M.M. supervised the work. All authors have contributed
285 and approved the final version of the manuscript.

286

287 **References**

- 288 1. Linder, J. & Robinson, J. W. A. Superconducting spintronics. *Nat. Phys.* **11**, 307–315 (2015).
- 289 2. Han, W., Maekawa, S. & Xie, X.-C. Spin current as a probe of quantum materials. *Nat. Mater.* **19**, 139–152
290 (2020).
- 291 3. Franke, K. J., Schulze, G. & Pascual, J. I. Competition of Superconducting Phenomena and Kondo Screening at
292 the Nanoscale. *Science* **332**, 940–944 (2011).
- 293 4. Malavolti, L. *et al.* Tunable Spin-Superconductor Coupling of Spin $\frac{1}{2}$ Vanadyl-Phthalocyanine Molecules.
294 *Nano Lett.* **18**, 7955–7961 (2018).
- 295 5. Nadj-Perge, S. *et al.* Observation of Majorana fermions in ferromagnetic atomic chains on a superconductor.
296 *Science* **346**, 602–607 (2014).
- 297 6. Bonizzoni, C. *et al.* Coherent coupling between Vanadyl Phthalocyanine spin ensemble and microwave
298 photons: towards integration of molecular spin qubits into quantum circuits. *Sci. Rep.* **7**, 13096 (2017).
- 299 7. Gimeno, I. *et al.* Enhanced Molecular Spin-Photon Coupling at Superconducting Nanoconstrictions. *ACS Nano*
300 **14**, 8707–8715 (2020).

- 301 8. Rogers, M. *et al.* Spin-singlet to triplet Cooper pair converter interface. *Commun. Phys.* **4**, 69 (2021).
- 302 9. Serrano, G. *et al.* Quantum dynamics of a single molecule magnet on superconducting Pb(111). *Nat. Mater.* **19**,
303 546–551 (2020).
- 304 10. Schwöbel, J. *et al.* Real-space observation of spin-split molecular orbitals of adsorbed single-molecule magnets.
305 *Nat. Commun.* **3**, 953 (2012).
- 306 11. Vitali, L. *et al.* Electronic Structure of Surface-supported Bis(phthalocyaninato) terbium(III) Single Molecular
307 Magnets. *Nano Lett.* **8**, 3364–3368 (2008).
- 308 12. Stepanow, S. *et al.* Spin and orbital magnetic moment anisotropies of monodispersed
309 bis(Phthalocyaninato)terbium on a copper surface. *J. Am. Chem. Soc.* **132**, 11900–11901 (2010).
- 310 13. Urdampilleta, M., Klyatskaya, S., Cleuziou, J.-P., Ruben, M. & Wernsdorfer, W. Supramolecular spin valves.
311 *Nat. Mater.* **10**, 502–6 (2011).
- 312 14. Thiele, S. *et al.* Electrical Readout of Individual Nuclear Spin Trajectories in a Single-Molecule Magnet Spin
313 Transistor. *Phys. Rev. Lett.* **111**, 037203 (2013).
- 314 15. Vincent, R., Klyatskaya, S., Ruben, M., Wernsdorfer, W. & Balestro, F. Electronic read-out of a single nuclear
315 spin using a molecular spin transistor. *Nature* **488**, 357–360 (2012).
- 316 16. Bogani, L. & Wernsdorfer, W. Molecular spintronics using single-molecule magnets. *Nat. Mater.* **7**, 179–186
317 (2008).
- 318 17. Urdampilleta, M., Klyatskaya, S., Ruben, M. & Wernsdorfer, W. Magnetic interaction between a radical spin
319 and a single-molecule magnet in a molecular spin-valve. *ACS Nano* **9**, 4458–4464 (2015).
- 320 18. Malavolti, L. *et al.* Magnetic Bistability in a Submonolayer of Sublimated Fe₄ Single-Molecule Magnets. *Nano*
321 *Lett.* **15**, 535–541 (2015).
- 322 19. Mannini, M. *et al.* Magnetic memory of a single-molecule quantum magnet wired to a gold surface. *Nat. Mater.*
323 **8**, 194–197 (2009).
- 324 20. Margheriti, L. *et al.* X-Ray Detected Magnetic Hysteresis of Thermally Evaporated Terbium Double-Decker
325 Oriented Films. *Adv. Mater.* **22**, 5488–5493 (2010).
- 326 21. Serrano, G. *et al.* Magnetic bistability of a TbPc₂ submonolayer on a graphene/SiC(0001) conductive
327 electrode. *Nanoscale* **10**, 2715–2720 (2018).
- 328 22. Wäckerlin, C. *et al.* Giant Hysteresis of Single-Molecule Magnets Adsorbed on a Nonmagnetic Insulator. *Adv.*
329 *Mater.* **28**, 5195–5199 (2016).
- 330 23. Malavolti, L. *et al.* Magnetism of TbPc₂ SMMs on ferromagnetic electrodes used in organic spintronics. *Chem.*
331 *Commun.* **49**, 11506–11508 (2013).

- 332 24. Mannini, M. *et al.* Magnetic behaviour of TbPc₂ single-molecule magnets chemically grafted on silicon surface.
333 *Nat. Commun.* **5**, 4582 (2014).
- 334 25. Sorrentino, A. L. *et al.* A TbPc₂ sub-monolayer deposit on Titanium Dioxide ultrathin film: a magnetic,
335 morphological, and chemical insight. *J. Mater. Chem. C* **9**, 15011–15017 (2021).
- 336 26. Gonidec, M. *et al.* Surface Supramolecular Organization of a Terbium(III) Double-Decker Complex on
337 Graphite and its Single Molecule Magnet Behavior. *J. Am. Chem. Soc.* **133**, 6603–6612 (2011).
- 338 27. Serrano, G. *et al.* Bilayer of Terbium Double-Decker Single-Molecule Magnets. *J. Phys. Chem. C* **120**, 13581–
339 13586 (2016).
- 340 28. Komeda, T., Isshiki, H., Liu, J., Katoh, K. & Yamashita, M. Variation of Kondo Temperature Induced by
341 Molecule–Substrate Decoupling in Film Formation of Bis(phthalocyaninato)terbium(III) Molecules on
342 Au(111). *ACS Nano* **8**, 4866–4875 (2014).
- 343 29. Serrano, G. *et al.* Substrate mediated interaction of terbium(iii) double-deckers with the TiO₂ (110) surface.
344 *Phys. Chem. Chem. Phys.* **23**, 12060–12067 (2021).
- 345 30. Cucinotta, G. *et al.* Tuning of a Vertical Spin Valve with a Monolayer of Single Molecule Magnets. *Adv. Funct.*
346 *Mater.* **27**, 1703600 (2017).
- 347 31. Diller, K. *et al.* Magnetic properties of on-surface synthesized single-ion molecular magnets. *RSC Adv.* **9**,
348 34421–34429 (2019).
- 349 32. Bozack, M. J. & Bryant, K. W. Elemental Lead by XPS. *Surf. Sci. Spectra* **1**, 324–327 (1992).
- 350 33. Pedrini, A. *et al.* Self-Assembly of TbPc₂ Single-Molecule Magnets on Surface through Multiple
351 Hydrogen Bonding. *Small* **14**, 1–7 (2017).
- 352 34. Powell, C. J. Recommended Auger parameters for 42 elemental solids. *J. Electron Spectros. Relat. Phenomena*
353 **185**, 1–3 (2012).
- 354 35. Pineda, E. M., Komeda, T., Katoh, K., Yamashita, M. & Ruben, M. Surface confinement of TbPc₂-SMMs:
355 structural, electronic and magnetic properties. *Dalt. Trans.* **45**, 18417–18433 (2016).
- 356 36. Studniarek, M. *et al.* Understanding the Superior Stability of Single- Molecule Magnets on an Oxide Film. *Adv.*
357 *Sci.* **6**, 1901736 (2019).
- 358 37. Poole, C. P., Farach, H. A., Creswick, R. J. & Prozorov, R. *Superconductivity*. (Elsevier Science, 2014).
- 359 38. Chanin, G. & Torre, J. P. Critical-Field Curve of Superconducting Lead. *Phys. Rev. B* **5**, 4357–4364 (1972).
- 360 39. Huebener, R. P. *Magnetic Flux Structures in Superconductors : Extended Reprint of a Classic Text*. (Springer
361 Berlin Heidelberg, 2001).
- 362 40. Prozorov, R., Giannetta, R. W., Polyanskii, A. A. & Perkins, G. K. Topological hysteresis in the intermediate

- 363 state of type-I superconductors. *Phys. Rev. B* **72**, 212508 (2005).
- 364 41. Prozorov, R. Equilibrium Topology of the Intermediate State in Type-I Superconductors of Different Shapes.
365 *Phys. Rev. Lett.* **98**, 257001 (2007).
- 366 42. Jeudy, V., Gourdon, C. & Okada, T. Impeded growth of magnetic flux bubbles in the intermediate state pattern
367 of type I superconductors. *Phys. Rev. Lett.* **92**, 147001 (2004).
- 368 43. Schawlow, A. L. & Devlin, G. E. Intermediate state of superconductors: Influence of crystal structure. *Phys.*
369 *Rev.* **110**, 1011–1016 (1958).
- 370 44. Huebener, R. P. & Kampwirth, R. T. Intermediate state structure in superconducting films of Indium. *Phys.*
371 *Status Solidi* **13**, 255–263 (1972).
- 372 45. Fortini, A. & Paumier, E. Thermodynamics of metastable processes in the magnetization of type-I
373 superconductors. *Phys. Rev. B* **14**, 55–60 (1976).
- 374 46. Prozorov, R. & Kogan, V. G. Effective Demagnetizing Factors of Diamagnetic Samples of Various Shapes.
375 *Phys. Rev. Appl.* **10**, 014030 (2018).
- 376 47. Atzori, M. *et al.* Room-Temperature Quantum Coherence and Rabi Oscillations in Vanadyl Phthalocyanine:
377 Toward Multifunctional Molecular Spin Qubits. *J. Am. Chem. Soc.* **138**, 2154–2157 (2016).
- 378 48. Camargo, L. C. *et al.* Exploring the Organometallic Route to Molecular Spin Qubits: The [CpTi(cot)] Case.
379 *Angew. Chemie* **133**, 2620–2625 (2021).
- 380 49. Végh, J. The analytical form of the Shirley-type background. *J. Electron Spectros. Relat. Phenomena* **46**, 411–
381 417 (1988).
- 382 50. Ohresser, P. *et al.* DEIMOS: A beamline dedicated to dichroism measurements in the 350–2500 eV energy
383 range. *Rev. Sci. Instrum.* **85**, 013106 (2014).
- 384 51. Nakajima, R., Stöhr, J. & Idzerda, Y. U. Electron-yield saturation effects in L -edge x-ray magnetic circular
385 dichroism spectra of Fe, Co, and Ni. *Phys. Rev. B* **59**, 6421–6429 (1999).
- 386 52. Brouder, C. Angular dependence of X-ray absorption spectra. *J. Phys. Condens. Matter* **2**, 701–738 (1990).
- 387 53. Cucinotta, G. pyDichroX. Available at: <https://github.com/BeppeC/pyDichroX>.
- 388

